ACTA ACUSTICA UNITED WITH ACUSTICA
Vol. 91 (2005) 671 – 679

Efficient FDTD-PE Model for Sound Propagation in Situations with Complex Obstacles and Wind Profiles

Timothy Van Renterghem[a], Erik M. Salomons[b], Dick Botteldooren[a]
[a] Ghent University, Department of Information Technology, Sint-Pietersnieuwstraat 41, B-9000 Gent, Belgium
[b] TNO TPD, P.O. Box 155, 2600 AD Delft, The Netherlands

Summary
An efficient hybrid model is presented for sound propagation in situations with several reflecting obstacles near the source. A Finite-Difference Time-Domain (FDTD) model is used in the complex source region, while a Parabolic Equation (PE) model is used for propagation to a distant receiver. The models are coupled by transformation of FDTD results at the boundary of the source region from the time domain to the frequency domain. The FDTD-PE model takes into account multiple reflections of sound waves in the source region, and interaction of sound waves with complex wind fields near the obstacles. It is shown that the FDTD-PE model is accurate, and requires considerably smaller computer times and memory than FDTD does.

PACS no. 43.20.El, 43.28.Fp, 43.28.Gq, 43.28.Js

1. Introduction

Noise barriers are widely used to reduce traffic noise. Accurate calculation of sound propagation over noise barriers is therefore of practical interest. Barriers cause reflection and diffraction of sound waves. In situations with barriers on both sides of a road, multiple reflections between the barriers occur. In addition, sound waves are refracted by wind and temperature gradients. Complex wind fields near noise barriers have a large effect on sound waves.

Sound propagation in situations with several reflecting obstacles and arbitrary wind and temperature fields can be modeled with a Finite-Difference Time-Domain (FDTD) model [1, 2, 3, 4, 5, 6]. The FDTD model is based on numerical integration of the linearized Euler equations in the time domain. A drawback of the FDTD model is that it requires large computer times and memory.

A more efficient model for outdoor sound propagation is the Parabolic Equation (PE) model [7, 8, 9, 10, 11]. The PE model is based on a one-way wave equation in the frequency domain. Consequently, the PE model is suitable for long-range sound propagation over flat ground, but less suitable for sound propagation in situations with several reflecting obstacles and arbitrary wind fields.

In many practical situations, *e.g.* a road with noise barriers, obstacles are located near the source while further away from the source there are no objects that significantly disturb the sound field. In these situations it is of interest to use a hybrid FDTD-PE model. FDTD is applied in the complex source region, while PE is used for propagation over flat ground to a distant receiver. In this way, computational efficiency is optimized.

In this article we present such a hybrid FDTD-PE model. Section 2 gives a general description of the coupling of FDTD, a time-domain model, to PE, a frequency-domain model. Section 3 describes the numerical implementation of the hybrid model. In section 4 we present FDTD-PE results for a number of test cases, and compare the results with results of other models (FDTD, GFPE, ray model). In this way we show that the FDTD-PE model is accurate. Complex atmospheric and acoustic effects, such as atmospheric turbulence and non-locally reacting ground reflection, are not included in the test cases, to keep the comparison as clear as possible. Section 5 discusses numerical efficiency of the FDTD-PE model, in terms of computer time and memory.

2. General approach

Figure 1 illustrates the basic approach of the FDTD-PE model. In the source region (gray area in the figure), with complex obstacles and complex wind fields, we use FDTD. The coupling of FDTD and PE occurs at a vertical array of intermediate receivers, located at the boundary of the source region. FDTD results at the intermediate receivers are used to generate starting functions for PE. Propagation to a distant receiver is computed with PE.

We use a 2D version of the FDTD model [1, 2], based on the 2D Euler equations. The source is represented by a broadband sound pulse. We calculate time signals of the

Received 17 July 2004,
accepted 30 December 2004.

sound pressure at the intermediate receivers. The computational domain of FDTD is chosen a little larger than the source region, so the boundary of the domain is not too close to the intermediate receivers. We allow for some space for so-called 'perfectly matched layers' [2, 12] at the top, right, and left boundaries of the computational domain, to simulate an unbounded atmosphere.

Spectral decomposition of the time signals yields starting functions for PE, for a wide range of frequencies at the same time. The vertical spacing of the intermediate receivers, and also the FDTD grid spacing, is chosen equal to the PE grid spacing for the highest frequency for which calculations are performed (*e.g.* one tenth of a wavelength). We use the Green's Function PE (GFPE) version of the PE model [9, 10, 11]. Since we use 2D FDTD, we also use 2D GFPE. Sound pressure levels at the distant receiver are transformed to relative levels by subtracting 'free-field' sound pressure levels, *i.e.* levels for an unbounded homogeneous atmosphere. In the appendix of this article we show that relative levels in 2D are equal to relative levels in 3D, in good approximation.

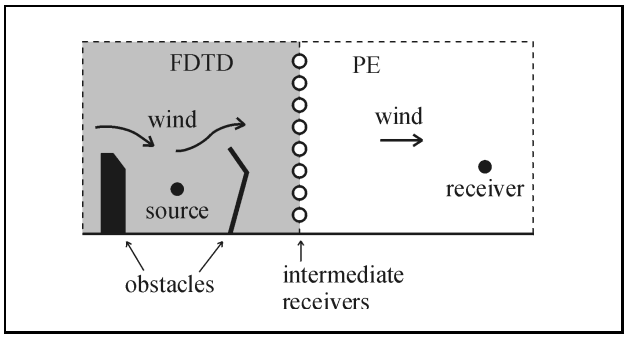

Figure 1. Schematic illustration of FDTD-PE model. FDTD is used in the source region (gray area), with complex obstacles and complex wind speed profiles. The FDTD computational domain is a little larger than the source region, so the intermediate receivers are located well within the FDTD computational domain. PE is used for propagation of the signals at the intermediate receivers to a distant receiver.

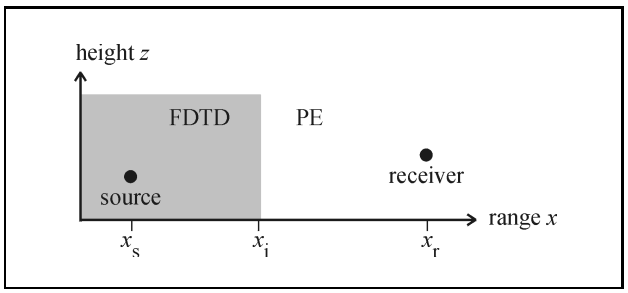

Figure 2. Geometry with xz coordinate system. The source region (gray area) extends to range x_i.

3. Implementation

This section describes details of the FDTD-PE model. We use the xz coordinate system shown in Figure 2. The source is located at range x_s and the receiver is located at range x_r. Intermediate receivers at the boundary of the source region are located at range x_i.

3.1. FDTD in the source region

In the source region we take into account not only reflection and diffraction by obstacles, but also refraction induced by complex wind fields around obstacles. Therefore, we first perform a CFD calculation with software package Fluent [13] to obtain a stationary background wind field for the FDTD calculation. The CFD calculation is based on Reynolds averaging, and employs an appropriate turbulence closure model.

For FDTD simulation of sound propagation *without* background flow (*i.e.* wind) it is advantageous to use a staggered grid, which means that acoustic pressure and acoustic velocity are discretized on mutually shifted subgrids [1, 2]. A staggered grid is used most naturally with a staggered time-integration scheme (pressure and velocity are updated at different times). In cases *with* background flow, however, the additional flow terms in the wave equations introduce some complications. Two options are found in the literature to solve this. Either one uses a collocated time-integration approach (pressure and velocity are updated at equal times) [5] or one uses the staggered time-integration approach in combination with a prediction step without background flow [2]. Both approaches have their own characteristics of memory use, computing times, numerical stability, and accuracy [14]. For this work we used the latter approach.

We use a computational grid with square cells. For the grid spacing δx we use a value of one tenth of the wavelength corresponding to the highest frequency of interest. The time step δt is chosen such that the 2D CFL number $\sqrt{2}c\delta t/\delta x$ is unity (c is the speed of sound). The FDTD model described above was validated by comparison with experimental data for various situations with noise barriers [12].

The surface of obstacles can be described by a surface impedance that is approximated in the time domain using a first order series expansion [15]. A more careful implementation of the ground surface is required for sound propagation over natural ground [16]. Alternatively, one may include a layer of absorbing ground material in the simulation domain [4, 12]. For the comparisons presented in this article, we assumed a rigid ground surface in the source region, thus avoiding the problem of the representation of the ground surface. Spurious reflections from the 'open' boundaries of the computational domain are eliminated by 'perfectly matched layers' [2, 12].

The FDTD calculation in the source region starts with a broadband sound pulse emitted by the source. We generate a Gaussian wavelet by adding to the sound pressure at the source position at each time step the time integral of the following function of time t

$$f(t) = A \sin\left[2\pi f_c(t-t_0)\right] \exp\left[-(t-t_0)^2/\sigma\right]$$

(so we add the sum $\sum f(t_j)\delta t$ over time levels t_j starting from $t_1 = 0$). Here A is a parameter related to the

amplitude of the pulse, f_c is a central frequency, t_0 is a time delay, and σ is a parameter related to the bandwidth $1/(2\sqrt{\sigma})$ of the pulse. It should be noted that one may also generate a starting pulse by assuming a Gaussian pressure distribution at $t = 0$ in a small region around the source position, for example; this approach yields identical *normalized* sound pressures (see section 3.5) as the approach described above does. Time signals of the sound pressure at all grid points at range $x = x_i$ (*i.e.*, at the intermediate receivers) are recorded.

3.2. FDTD outside the source region

In this work, propagation outside the source region is calculated with PE. However, for the sake of comparison of the computational efficiency of models (in section 5), an efficient 'moving-window' implementation of FDTD [4] outside the source region is briefly discussed in this section.

We assume that outside the source region the one-way propagation approximation is valid, which is required for application of PE. This implies that the efficient moving-window implementation of FDTD can be used, at least if we have a short pulse-like signal traveling through the atmosphere. By restricting the computational grid to a moving window that follows the pulse, the number of grid cells that must be kept in memory is reduced. Grid cells outside the window can be ignored since the field is zero at these cells. In this way, computer times and memory can be very much reduced. If the pulse is smeared out over a longer time, for example owing to multiple reflections between parallel noise barriers (see section 4), the moving-window approach loses its efficiency.

3.3. Transition from FDTD to PE

To generate starting functions for PE, the FDTD time signals are transformed by FFT to the frequency domain. This gives starting functions of the complex sound pressure $p(z_j)$ sampled at grid points $j = 1, 2, \ldots$ at $x = x_i$, for a range of frequencies covered by the broadband sound pulse.

Some manipulations are required to adjust the starting functions $p(z_j)$ to the PE grid, for two reasons:

1. the PE vertical grid spacing δz is one tenth of a wavelength and therefore varies with frequency, while $p(z_j)$ from FDTD is sampled at one tenth of the wavelength corresponding to the highest frequency,
2. the PE grid may be higher than the FDTD grid.

The first point is solved by interpolation of the starting function $p(z_j)$ at the PE grid points. The second point is solved by extrapolation of the starting function $p(z_j)$ to the top of the PE grid. We used the following approach: linear extrapolation of the phase angle of p and linear tapering to zero of the magnitude of p.

We enforce continuity of the sound pressure but not of the acoustic velocity at the transition, as PE employs only the sound pressure as an independent variable. It is not obvious that this approach gives accurate results. The numerical test calculations presented in section 4 show, however, that the results are accurate. In principle, the coupling of FDTD and PE may also be disturbed by the one-way propagation approximation of PE, the angular limitation of PE, and the absorbing top layers employed with FDTD and PE. These points should be taken into account in the choice of the computational domains of FDTD and PE.

3.4. PE

We use a 2D GFPE model, which is closely related to the axisymmetric 3D GFPE model described in Refs. [9, 10, 11]. The 3D model is based on transformation of the complex pressure p to the variable $q = p\sqrt{r}$, where r is propagation range. For an axisymmetric system, the 3D Helmholtz equation for p corresponds to a 2D Helmholtz equation for q, which is transformed into a parabolic equation for one-way sound propagation. So by using $q = p$ instead of $q = p\sqrt{r}$, we obtain a 2D GFPE model.

A PE calculation starts with a starting function, which is provided by FDTD in this case. The starting function is extrapolated stepwise in positive x direction on a grid with rectangular cells (x is equal to range r indicated above). The vertical grid spacing is one tenth of a wavelength, while the horizontal grid spacing may be several wavelengths [9, 10, 11]. At the top of the PE grid an absorbing layer is used to prevent spurious reflections. Atmospheric wind is taken into account by using the effective sound speed approximation. The ground is modeled by a complex, frequency-dependent impedance. The output of a PE calculation is the complex sound pressure at the receiver.

3.5. Relative sound pressure levels

Finally the 2D PE results are converted to relative sound pressure levels (relative SPL), *i.e.* sound pressure levels relative to free field:

$$\Delta L = 20 \lg \left(|p| / |p_{\mathrm{free}}| \right),$$

where p is the complex sound pressure at the receiver and p_{free} is the free-field complex sound pressure at the receiver.

The free field is calculated as follows. First a 'free' FDTD signal is recorded at a short distance r_0 from the source (typically $r_0 = 5\,\mathrm{m}$). Source and receiver are located far from all boundaries in this calculation. Application of FFT to the 'free' signal yields the complex sound pressure $p_{\mathrm{free},0}$ at distance r_0. Next $|p_{\mathrm{free}}|$ is calculated by the relation

$$|p_{\mathrm{free}}| = |p_{\mathrm{free},0}| |H_0^{(1)}(kr) / H_0^{(1)}(kr_0)|,$$

where k is the wave number and $H_0^{(1)}$ is the Hankel function of order zero and the first kind (*i.e.* the Green's function for a point source in 2D, or a coherent line source in 3D). This relation can be simplified by using the far-field expansion of the Hankel function:

$$|p_{\mathrm{free}}| = |p_{\mathrm{free},0}| \sqrt{r_0 / r}.$$

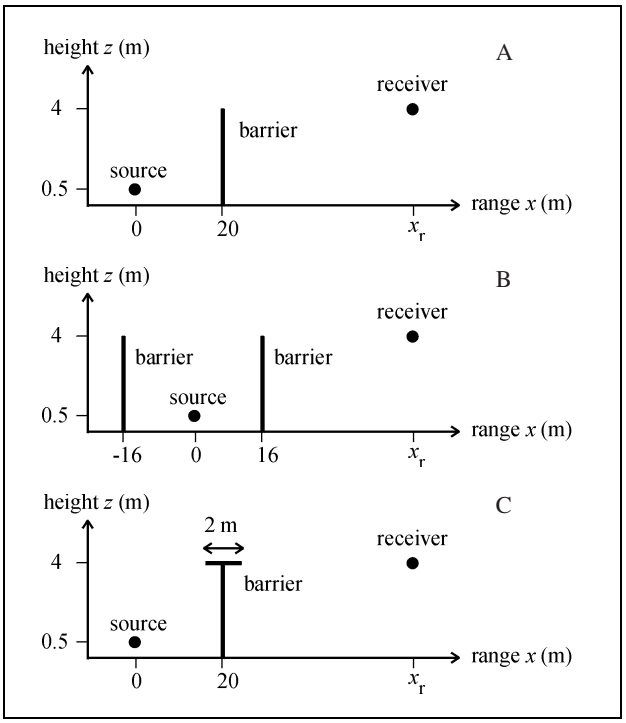

Figure 3. Geometry A with a single noise barrier, geometry B with two noise barriers and geometry C with a single noise barrier with a T-top.

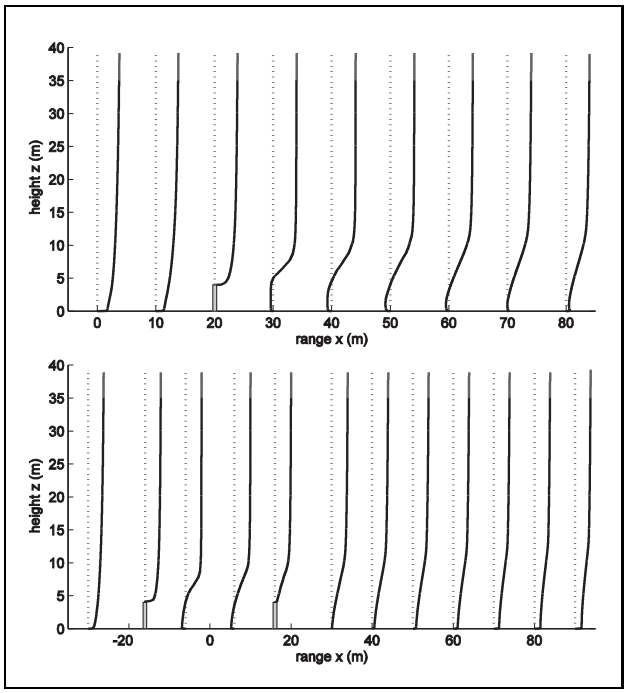

Figure 4. Vertical profiles of the horizontal wind speed component calculated with Fluent for test case 2 (top) and test case 4 (bottom).

Table I. Specification of five test cases. x_i: FDTD-PE transition range.

case	geometry	x_i [m]	wind
1	A	24	no wind
2	A	24	wind from source to receiver
3	B	21	no wind
4	B	21	wind from source to receiver
5	C	24	wind from source to receiver

4. Numerical examples

In this section we present results of calculations with the FDTD-PE model for five test cases, and we compare the results with results from other models.

4.1. Test cases

The test cases are specified in Table 1, with geometries A, B, and C represented in Figure 3. In cases 1 and 2 we have a single noise barrier between source and receiver (geometry A), without and with wind, respectively. In cases 3 and 4 we have noise barriers on both sides of the source (geometry B), without and with wind, respectively. In case 5 we have a single barrier with a 2 m wide T-top (geometry C) and with wind.

In all cases the source is located at range $x_s = 0$ and height 0.5 m. The receiver height is 4 m, and the receiver range x_r varies between zero and 500 m. The noise barriers are 4 m high, and have a thickness of 0.1 m. The surface of the barriers is rigid.

The ground surface up to the FDTD-PE transition point x_i (see Table I) is rigid. For the ground surface beyond this point we consider both rigid ground and absorbing ground. For absorbing ground we used the Delany and Bazley impedance model [17] with a flow resistivity of 200 kPa s m^{-2}, a value typical for grassland. The absorbing ground will be referred to as grassland.

As a test of the accuracy of the FDTD-PE model, FDTD-PE results were compared with FDTD results, *i.e.* results from calculations with FDTD applied for the entire propagation path from source to receiver. For grassland no FDTD calculations were performed for the reason mentioned in section 3.1.

Wind profiles for test cases 2, 4, and 5 were calculated with CFD software package Fluent [13]. Figure 4 shows the profiles of the horizontal wind speed component for test cases 2 and 4. For the flow calculations we used a logarithmic inflow profile $u(z) = (u*/\kappa)\ln(z/z_0)$, with friction velocity $u* = 0.4$ m/s, von Kármán constant $\kappa = 0.4$, and ground roughness length $z_0 = 0.01$ m. This profile corresponds to wind directed from source to receiver, so we have downwind sound propagation. We further used the $k\varepsilon$ turbulence model, standard wall functions, and a smooth ground surface (except for the inflow profile). A homogeneous temperature distribution was assumed.

4.2. Computational parameters

The FDTD computational domain used for the calculations was $\{-3\,\text{m} < x < 27\,\text{m}, 0\,\text{m} < z < 42\,\text{m}\}$ for cases 1, 2, and 5 (single noise barrier), $\{-19\,\text{m} < x < 24\,\text{m}, 0\,\text{m} < z < 42\,\text{m}\}$ for cases 3 and 4 (two noise barriers).

We used a grid spacing of 0.05 m and a time step of 0.1 ms. For the Gaussian wavelet emitted by the source we used the parameters $A = 104\,\mathrm{Pa/s}$, $t_0 = 0.02\,\mathrm{s}$, $f_c = 300\,\mathrm{Hz}$, and $\sigma = 10^{-5}\,\mathrm{s}^2$ (corresponding to a bandwidth of 158 Hz). The absorbing layers at the boundaries of the domain consisted of 40 computational cells, and absorption parameters were optimized such that a sound wave is reduced by 120 dB upon reflection at normal incidence.

The FDTD time signals should be long enough to capture all significant reflections in the source region. For cases 1, 2, and 5 (single noise barrier), a length of 2500 time steps (0.25 s) was sufficient. For cases 3 and 4 (two noise barriers), a length of 8000 time steps (0.8 s) was required to capture all significant reflections between the barriers. Before application of the FFT algorithm, we extended the signals by 'zero padding' to make the number of samples a power of 2.

We performed PE calculations for three frequencies: 100, 300, and 500 Hz.

Vertical grid spacings were 0.3, 0.1, and 0.06667 m, respectively. For the horizontal grid spacing we use a constant value of 1 m (this value may be optimized [9, 10, 11]). For all frequencies, the height of the PE grid was 2048 grid spacings, including an absorbing top layer of 500 grid spacings.

4.3. PE starting functions

As an example, Figure 5 shows the magnitude of the starting function $p(z)$ for PE as calculated with FDTD for case 1 and frequencies 100, 300, and 500 Hz. The sharp decay of the magnitude in the height interval between 40 m and 42 m is due to the absorbing top layer in FDTD. The starting functions were adjusted to the PE grid by interpolation and extrapolation as described in section 3.

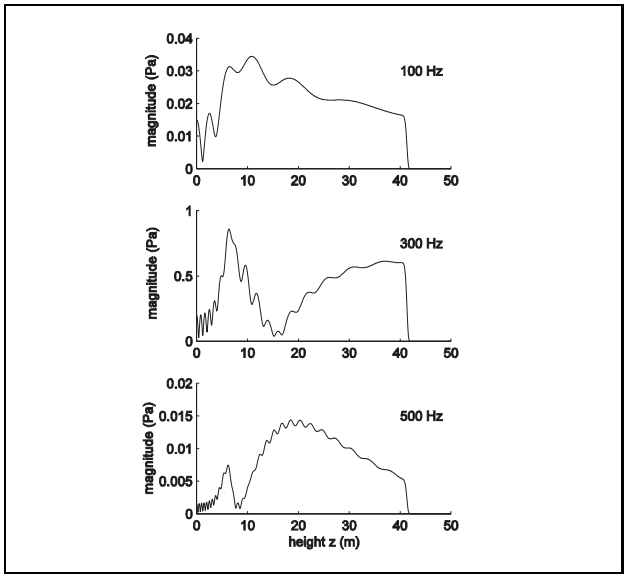

Figure 5. Magnitude of starting functions $p(z)$ for PE as calculated with FDTD for case 1 and frequencies 100, 300, and 500 Hz (not including the extrapolation indicated in section 3.3).

4.4. Results

Results for test cases 1 to 5 are shown in Figures 6 to 10, respectively. The graphs show FDTD-PE results up to a range of 500 m, for rigid ground (graphs on the left) and for grassland for $x > x_i$ (graphs on the right). The graphs for rigid ground also show FDTD results up to a range of 150 m.

For case 1 with rigid ground we also included results of a ray model based on the theory of diffraction [18]. For case 2 with rigid ground we also included results of the PE model, using the Kirchhoff approximation for the effect of the noise barrier [19].

For the cases without wind (cases 1 and 3), the agreement between FDTD and FDTD-PE is excellent. For the cases with wind (cases 2, 4, and 5), the agreement is good, with differences less than 1 dB except near interference minima.

For case 1 we have good agreement between the ray model and FDTD-PE. The ray model is 3D, so the agreement confirms that relative levels in 2D are equal to relative levels in 3D, in good approximation.

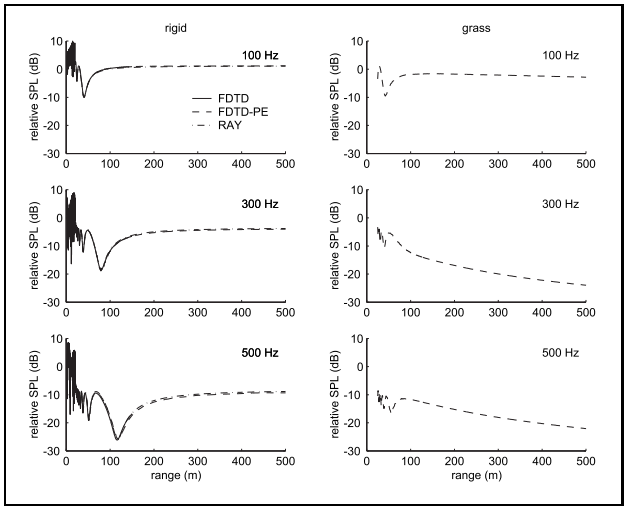

Figure 6. Relative sound pressure level (relative SPL) calculated with FDTD and FDTD-PE for test case 1. Graphs on the left are for rigid ground and graphs on the right are for grassland for $x > x_i$. For comparison, results of a 3D ray model are also included.

For case 2 we see that PE results deviate a bit from FDTD-PE results and FDTD results. The origin of this deviation is probably the use of the Kirchhoff approximation for the effect of the noise barrier with PE.

Comparison of FDTD-PE results for cases 1 and 3 shows that the barrier on the left of the source (see Figure 3b) considerably enhances the sound levels at 300 and 500 Hz. In other words, the barrier on the right is less effective for sound waves reflected by the barrier on the left than for direct sound waves. Comparison of FDTD-PE results for cases 2 and 5 shows that the effect of the T-top in case 5 is small.

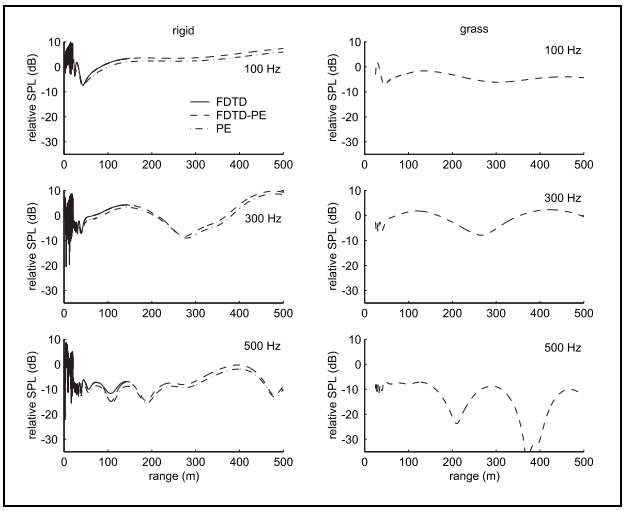

Figure 7. As Figure 6, for test case 2. For comparison, PE results are also included.

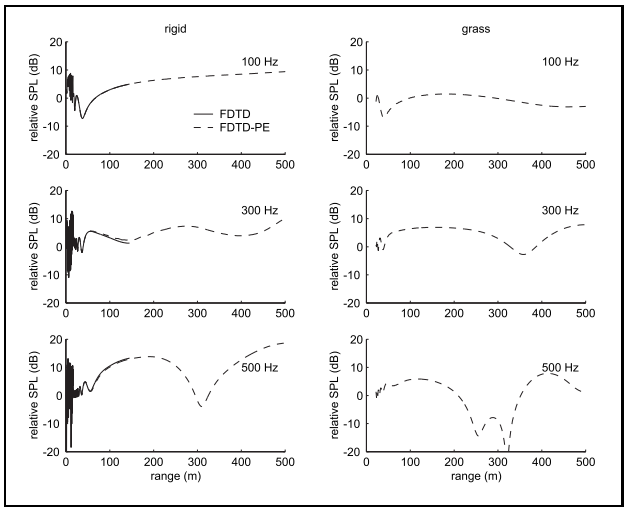

Figure 9. As Figure 6, for test case 4.

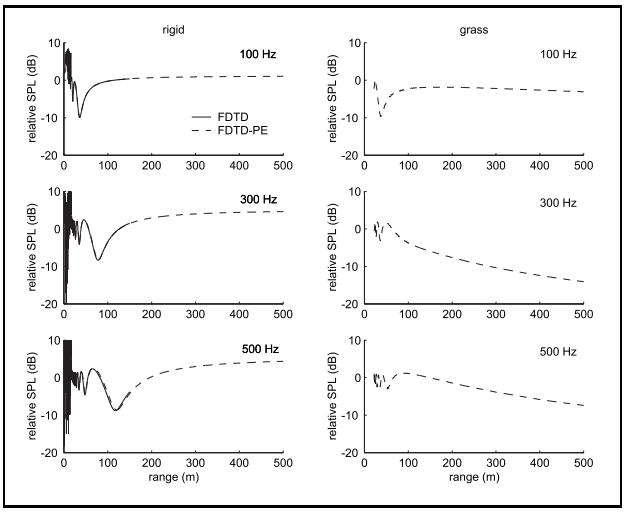

Figure 8. As Figure 6, for test case 3.

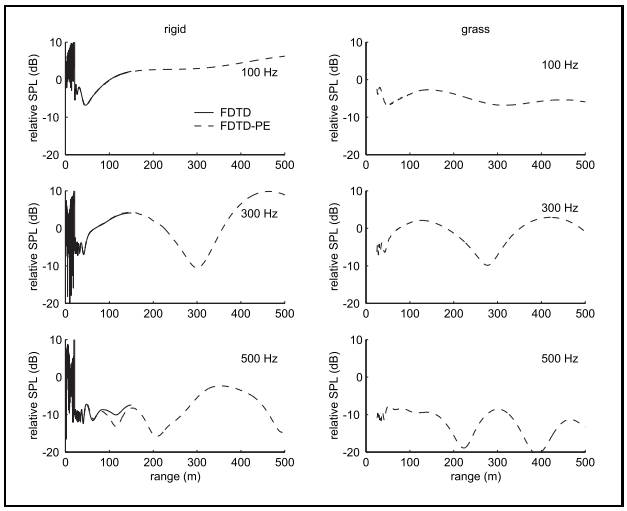

Figure 10. As Figure 6, for test case 5.

Comparison of FDTD-PE results for cases 1 and 2, and cases 3 and 4, shows that the effect of wind is large, in particular for grassland. The low levels for grassland without wind are due to destructive interference between direct sound from the barrier top to the receiver and sound reflected by the ground surface between the barrier and the receiver. Wind disturbs this destructive interference. In addition, the paths of sound waves in a downward refracting atmosphere are curved downward, so the barrier on the right is less effective in cases with wind than in cases without wind.

5. Efficiency of FDTD and PE calculations

In this section we discuss efficiency of the FDTD, PE, and FDTD-PE models, in terms of computer time and memory. For this study we used the GFPE implementation of the PE model, but computer time and memory is of the same order of magnitude as for the CNPE implementation, although GFPE may be a little faster than CNPE [7, 8, 9, 10, 11].

5.1. Memory

For a FDTD calcul ation we use a grid with $M_{\mathrm{FDTD}} \times N_{\mathrm{FDTD}}$ square cells. We assume cell dimensions of one tenth of a wavelength: $\delta x = 0.1\lambda$ and $\delta z = 0.1\lambda$. The vertical number of cells is given by $M_{\mathrm{FDTD}} = z_{\max}/\delta z$, where $z_{\max}$ is the height of the grid. The horizontal number of cells is $N_{\mathrm{FDTD}} = R/\delta x$, where R is the horizontal size of the grid, which is of the order of the horizontal distance between the source and the receiver. An FDTD calculation requires storage of approximately $n_{\mathrm{FDTD}} M_{\mathrm{FDTD}} N_{\mathrm{FDTD}}$ numbers, where n_{FDTD} is the number of variables that must be specified at all grid points, including variables for storage of intermediate results. Without background flow we need only three variables: pressure, horizontal velocity, and vertical velocity, so n_{FDTD} is 3. With background flow, additional variables have to be stored to obtain sufficient accuracy. With the collocated time-integration approach n_{FDTD} is 6, since the variables are stored at two time levels. With the staggered time-integration approach with prediction step, n_{FDTD} is

4 [14]. The latter approach is used here. Let us consider an example. For $R = 100\,\mathrm{m}$, $\lambda = 1\,\mathrm{m}$, $n_{\mathrm{FDTD}} = 4$, and $M_{\mathrm{FDTD}} = 1000$, 4 million numbers have to be stored. In practice, the amount of numbers may be larger for the sake of computational speed and flexibility of the code. Also, a full sound speed field or wind speed field as in test cases 2, 4, and 5 in section 4 requires storage of up to three additional variables.

For GFPE we use a grid with $M_{\mathrm{PE}} \times N_{\mathrm{PE}}$ rectangular cells. The field is calculated by stepwise extrapolation in the positive x-direction of the field at a column of grid points. As for FDTD, we assume a vertical cell size $\delta z = 0.1\lambda$. The horizontal cell size (or extrapolation step size) is $\delta x = a\lambda$, where a varies roughly between 5 and 50 [9, 10]. A GFPE calculation requires storage of approximately $n_{\mathrm{PE}} 2M_{\mathrm{PE}}$ numbers, where n_{PE} is the number of variables that must be specified at all grid points of the column, and the factor 2 reflects that GFPE uses FFT's of length $2M_{\mathrm{PE}}$. The number of variables n_{PE} is 9 in our GFPE implementation, including the field itself and some precalculated vectors used to speed up the extrapolation of the field. For example, for $n_{\mathrm{PE}} = 9$ and $M_{\mathrm{PE}} = 2048$ we have to store about 36 thousand numbers. This is a factor of about 100 smaller than the 4 million numbers to be stored for FDTD.

The precise amounts of memory required for FDTD and PE depend on the implementations, but it is obvious that FDTD requires much more memory than PE does. The reason for this is that FDTD holds in memory the acoustic field at all cells of the grid, while PE holds in memory the acoustic field at a single column that is extrapolated stepwise through the grid.

The large memory required for FDTD can be reduced by using a 'moving window' that follows a sound pulse traveling through the atmosphere [4], as explained in section 3.2. This approach is only efficient if the sound pulse at the receiver is sufficiently short, such as in cases 1, 2, and 5 with a single noise barrier. In cases 3 and 4, however, the sound signal at the receiver is long due to multiple reflections between the two barriers, so the moving-window approach is not efficient.

With the hybrid FDTD-PE model, we keep computer memory small by using FDTD only in the source region. Since the amount of numbers to be stored with FDTD is proportional to the total number of cells in the grid, the memory required for FDTD-PE can be kept much smaller than the memory required for FDTD.

5.2. Computational speed

Comparison of the computational speeds of FDTD and PE is difficult, since computing times depend strongly on the implementation of the models. To get an impression, however, we compared computing times of a C++ implementation of FDTD and a Matlab implementation of PE, both running on a Pentium IV PC. The Matlab PE code employs a built-in C-routine for the time-consuming evaluation of the FFT. Using the computational parameters given in section 4.2, we found that the FDTD computing time is larger than the PE computing time by a factor of approximately $17n + 250$ without background flow and $10(17n + 250)$ with background flow, where n is the propagation distance expressed in wavelengths. The offset for $n = 0$ corresponds to the time needed to prepare various variables before the actual calculation starts. For large n, the speed ratio increases linearly with distance n. This corresponds to a quadratic increase of FDTD computing time and a linear increase of PE computing time with n (assuming that the height of the computational grid is kept constant). For a frequency of 500 Hz and a propagation distance of 100 m, the speed ratio is 2750 without flow and 27500 with flow. It should be noted that the speed ratio can be reduced considerably by using the efficient moving-window implementation of FDTD.

The expressions for the speed ratio given above apply to a calculation for a single frequency. A major advantage of FDTD, however, is that it works in the time domain, so a full spectrum can be obtained from a single calculation for a broadband sound pulse. For a spectrum with 100 frequencies, for example, the speed ratio between PE and FDTD is reduced by a factor of 100.

With the hybrid FDTD-PE model, we keep computing times small by using FDTD only in the source region. FDTD computing times increase with the square of propagation distance, so FDTD-PE is much faster than FDTD except for small distances.

6. Conclusions

The FDTD-PE model presented in this article is useful for situations with several obstacles near the source, such as a road with noise barriers on both sides, or an industrial site with noise sources surrounded by barriers and buildings. Results of the model for five test cases agree well with results of other models. This confirms that the coupling of FDTD and PE by transformation from the time domain to the frequency domain works well.

Computer times and memory use are much larger for FDTD than for PE. Consequently, FDTD-PE is a more efficient model than FDTD, for situations in which obstacles and complex flow are localized in a small region around the source, so that PE can be applied in the large region outside the source region.

The FDTD-PE model used for this work is a 2D model, but it has been shown that relative sound pressure levels in 2D are equal to relative sound pressure levels in 3D, in good approximation. Application of FDTD-PE in 3D does not appear feasible on common computers in the near future, except for situations with small source regions or very low frequencies.

Appendix
Relative sound pressure levels in 2D and 3D

Objective

In this appendix we show that 2D calculations can be used for predicting sound levels generated by a point source in

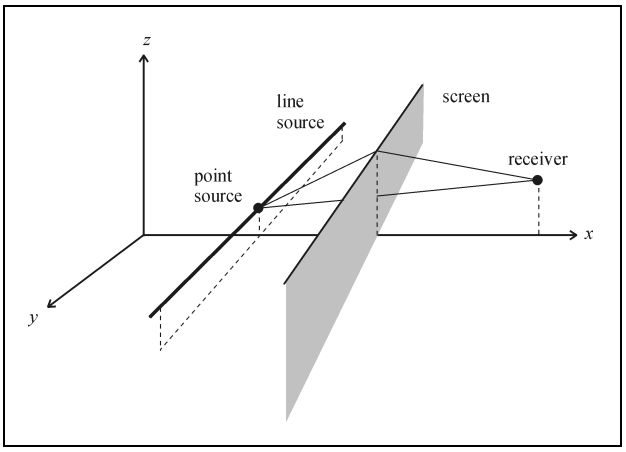

Figure A1. 3D representation in perspective of a situation with a line source, a screen, and a receiver. Line source and screen are parallel to the y axis.

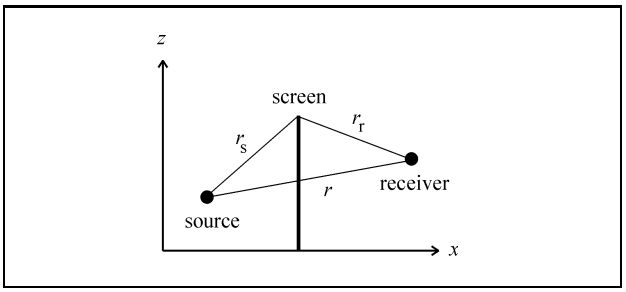

Figure A2. 2D cross-section of Figure A1 in the xz plane. Distances r_s, r_r, and r in the xz plane are indicated.

3D. We first consider the geometry shown in Figures A1 and A2, with a homogeneous atmosphere, a single noise screen, and no ground surface (the screen extends down to $z = -\infty$). The more general case with several reflecting obstacles and a reflecting ground surface is discussed in the last paragraph below.

For simplicity, we choose the origin of the xyz coordinate system shown in Figure A1 at the screen top, so we have the following positions:

- source (x_s, y_s, z_s),
- receiver $(x_r, y_r = 0, z_r)$,
- screen top $(x = 0, y, z = 0)$, with $-\infty < y < \infty$.

For the line source shown in Figure A1 we have $-\infty < y_s < \infty$. For the point source we have $y_s = 0$.

If we perform a 2D calculation in the xz plane with a point source (Figure A2), we are effectively simulating the 3D system with the line source. We are interested, however, in the 3D system with the point source.

We will show that the relative SPL (*i.e.* SPL relative to free field; see section 3.5) generated by the line source is a very good approximation of the relative SPL generated by the point source at $y_s = 0$:

$$\Delta L_2 \approx \Delta L_3(y_s = 0). \tag{A1}$$

Here, ΔL_2 is the relative SPL of the line source, obtained from a 2D calculation, and $\Delta L_3(y_s = 0)$ is the relative SPL of the point source at $y_s = 0$.

Sound field of point source and line source

The (diffracted) sound pressure generated by the point source at arbitrary y_s can be written as

$$p_3 = D\frac{\mathrm{e}^{\mathrm{i}kR_d}}{R_d}. \tag{A2}$$

Here D is a spherical-wave diffraction coefficient (derived from the diffraction theory of Hadden and Pierce, for example; see [18]), k is the wave number, and R_d is the length of the diffracted sound ray from the source to the receiver:

$$R_d = \sqrt{r_d^2 + y_s^2}, \tag{A3}$$

where $r_d = r_s + r_r$ is the length of the diffracted sound ray in the plane perpendicular to the screen, with $r_s = \sqrt{x_s^2 + z_s^2}$ and $r_r = \sqrt{x_r^2 + z_r^2}$ (see Figure A2).

The sound pressure generated by the line source follows by integration over y_s:

$$p_2 = \int_{-\infty}^{\infty} p_3 \,\mathrm{d}y_s, \tag{A4}$$

as can be verified by substitution into the inhomogeneous 2D Helmholtz equation [4]. The relative SPL of the line source is

$$\Delta L_2 = 20\lg\left(\frac{|p_2|}{|p_{2,\mathrm{free}}|}\right), \tag{A5}$$

with $p_{2,\mathrm{free}} = \mathrm{i}\pi H_0^{(1)}(kr)$,
where $r = \sqrt{(x_r - x_s)^2 + (z_r - z_s)^2}$ is the distance from the line source to the receiver. The relative SPL of the point source is

$$\Delta L_3 = 20\lg\left(\frac{|p_3|}{|p_{3,\mathrm{free}}|}\right), \tag{A6}$$

with $p_{3,\mathrm{free}} = \exp(\mathrm{i}kR)/R$, where $R = \sqrt{y_s^2 + r^2}$ is the distance from the point source to the receiver.

Proof

In this section we give a proof of equation (A1). We evaluate the integral in equation (A4) with the *method of stationary phase* (see [11], for example). This method applies for large wave number k (in this case $k_r d \gg 1$), and is therefore consistent with the geometrical-acoustics approximation.

The point of stationary phase is at $y_s = 0$. We find:

$$p_2 = D_0\sqrt{\frac{2\pi}{kr_d}}\exp(\mathrm{i}kr_d + \mathrm{i}\pi/4), \tag{A7}$$

with $D_0 \equiv D(y_s = 0)$. Analogously, we find the following stationary-phase approximation of the free-field sound pressure $p_{2,\mathrm{free}} = \int_{-\infty}^{\infty} p_{3,\mathrm{free}} \,\mathrm{d}y_s$:

$$p_{2,\mathrm{free}} = \sqrt{\frac{2\pi}{kr}}\exp(\mathrm{i}kr + \mathrm{i}\pi/4). \tag{A8}$$

This expression agrees with the asymptotic form of $p_{2,\mathrm{free}} = \mathrm{i}\pi H_0^{(1)}(kr)$ for large k, using equation 9.2.3 from [20].

From equations (A7) and (A8) we find the following expression for the normalized sound pressure of the line source:

$$\frac{p_2}{p_{2,\mathrm{free}}} = D_0\sqrt{\frac{r}{r_d}}\exp(\mathrm{i}kr_d - \mathrm{i}kr). \tag{A9}$$

The corresponding relative SPL is

$$\Delta L_2 = 20\lg\left(|D_0|\sqrt{\frac{r}{r_d}}\right). \tag{A10}$$

The normalized sound pressure of the point source at $y_s = 0$ is

$$\frac{p_3}{p_{3,\mathrm{free}}} = D_0\frac{r}{r_d}\exp(\mathrm{i}kr_d - \mathrm{i}kr). \tag{A11}$$

The corresponding relative SPL is

$$\Delta L_3 = 20\lg\left(|D_0|\sqrt{\frac{r}{r_d}}\right). \tag{A12}$$

The phase angles of the normalized sound pressures given by equations (A9) and (A11) are equal, and the amplitudes differ by a factor $\sqrt{r/r_d}$. The factor $\sqrt{r/r_d}$ is close to unity in most practical situations (while $|D_0|$ is not close to unity, in general), so we find that equation (A1) holds.

General case

In general, we have several reflecting obstacles and a reflecting ground surface. We use the geometrical-acoustics approximation: the sound pressure at the receiver is equal to the sum of contributions from all sound rays. Each contribution is of the form of equation (A.2), with diffraction coefficient D replaced by a product of diffraction coefficients and reflection coefficients. The product corresponds to the various diffractions and reflections along the sound ray. With this replacement, the derivation given in section A.3 applies to each sound ray. After summation we find, with the approximation $\sqrt{r/r_d} \approx 1$, that equation (A1) holds also in the general case.

References

[1] D. Botteldooren: Acoustical finite-difference time-domain simulation in a quasi-Cartesian grid. J. Acoust. Soc. Am. **95** (1994) 2313–2319.

[2] T. Van Renterghem: The finite-difference time-domain method for simulation of sound propagation in a moving medium. PhD thesis, University Gent, 2003.

[3] R. Blumrich, D. Heimann: A linearized eulerian sound propagation model for studies of complex meteorological effects. J. Acoust. Soc. Am. **112** (2002) 446–455.

[4] E. M. Salomons, R. Blumrich, D. Heimann: Eulerian time-domain model for sound propagation over a finite-impedance ground surface. comparison with frequency-domain models. Acta Acustica united with Acustica **88** (2002) 483–492.

[5] D. K. Wilson, M. L. Moran, L. Liu, V. E. Ostashev, D. F. Aldridge, N. P. Symons, D. H. Marlin: Development of a high-fidelity simulation capability for battlefield acoustics. SPIE AeroSense meeting 2003, Orlando, Florida, 2003.

[6] V. E. Ostashev, L. Liu, D. K. Wilson, M. L. Moran, D. F. Aldridge, D. Marlin: Starting equations for direct numerical simulation of sound propagation in the atmosphere. Proc. 10th International Symposium on Long Range Sound Propagation, Grenoble, France, 2002.

[7] K. E. Gilbert, M. J. White: Application of the parabolic equation to sound propagation in a refracting atmosphere. J. Acoust. Soc. Am. **85** (1989) 630–637.

[8] M. West, K. E. Gilbert, R. A. Sack: A tutorial on the parabolic equation (PE) model used for long range sound propagation in the atmosphere. Applied Acoustics **37** (1992) 31–49.

[9] K. E. Gilbert, X. Di: A fast Green's function method for one-way sound propagation in the atmosphere. J. Acoust. Soc. Am. **94** (1993) 2343–2352.

[10] E. M. Salomons: Improved Greens function parabolic equation method for atmospheric sound propagation. J. Acoust. Soc. Am. **104** (1998) 100–111.

[11] E. M. Salomons: Computational atmospheric acoustics. Kluwer, Dordrecht, 2001.

[12] T. Van Renterghem, D. Botteldooren: Numerical simulation of the effect of trees on downwind noise barrier performance. Acta Acustica united with Acustica **89** (2003) 764–778.

[13] Fluent: Computational fluid dynamics software, version 6. Fluent, Incorporated, Centerra Resource Park, 10 Cavendish Court, Lebanon, NH 03766.

[14] T. Van Renterghem, D. Botteldooren, E. M. Salomons: Efficiency of FDTD and hybrid techniques for outdoor sound propagation modeling. Proceedings of Long Range Sound Propagation Symposium, Fairlee, Vermont, USA, 2004.

[15] D. Botteldooren: Finite-difference time-domain simulation of low-frequency room acoustic problems. J. Acoust. Soc. Am. **98** (1995) 3302–3308.

[16] K. Heutschi, M. Horvath, J. Hofmann: Simulation of ground impedance in finite difference time domain calculations of outdoor sound propagation. Acta Acustica united with Acustica **91** (2005) 35–40.

[17] M. E. Delany, E. N. Bazley: Acoustic properties of fibrous absorbent materials. Applied Acoustics **3** (1970) 105–116.

[18] E. M. Salomons: Sound propagation in complex outdoor situations with a non-refracting atmosphere: model based on analytical solutions for diffraction and reflection. Acta Acustica united with Acustica **83** (1997) 436–454.

[19] E. M. Salomons: Diffraction by a screen in downwind sound propagation: a parabolic-equation approach. J. Acoust. Soc. Am. **95** (1994) 3109–3117.

[20] M. Abramowitz, I. A. Stegun (eds.): Handbook of mathematical functions. Dover, New York, 1972.